Journal of Intelligent Material Systems and Structures OnlineFirst, published on March 19, 2010 as doi:10.1177/1045389X10366316

Electro-rheological Cylinders used as Impact Energy Absorbers

X. W. ZHANG,[1] T. X. YU[1,]* AND W. J. WEN[2]

[1]Department of Mechanical Engineering, Hong Kong University of Science and Technology Clear Water Bay, Kowloon, Hong Kong, China

[2]Department of Physics, Hong Kong University of Science and Technology, Clear Water Bay, Kowloon, Hong Kong, China

ABSTRACT: Smart fluids, that is, electro-rheological (ER) and magneto-rheological (MR) fluids have been studied widely in vibration control, seismic isolations, and rotation transmission, where the velocity is low and the motions are periodic. However, very few investigations concern about the dynamic response and energy absorption of ER dampers under impact loadings. To explore the feasibility of using ER cylinders as impact energy absorbers, two different ER fluids were first characterized by using a capillary rheometer with rectangular duct. Then, a double-ended ER cylinder with two parallel annular ducts was designed, and its performance in response to a mass impact was tested. The experiments show that a typical dynamic response of the ER cylinder consists of three distinct stages, namely, an initial shock stage, a transition stage, and a stable flow stage. Afterwards, the dynamic response is analyzed theoretically, in which the contact between the impinger and the piston rod, the viscous and ER effects as well as the inertia and response time of the ER fluid are considered. It is revealed that, the controllability of the ER impact energy absorber greatly depends on the impact velocity and ER fluid's yield stress, and that when the impact velocity increases, its controllability deteriorates due to viscosity and response time.

Key Words: electro-rheological, characterization, response time, impact, energy absorbers.

INTRODUCTION

SMART fluids, including electro-rheological (ER) and magneto-rheological (MR) fluids, are special suspensions which consist of large mounts of solid particles dispensed in certain carrier liquids. When subjected to a high-intensity electric or magnetic field, the flow properties of these fluids can be changed promptly and this process is reversible. Therefore, the flow resistance of the smart fluids can be controlled by adjusting the intensity of applied electric/magnetic field. Due to their fast response and controllability, the smart fluids have attracted great attentions of engineers and researchers since their inventions (Wang and Meng, 2001; Stanway, 2004). In the past decades, the applications of these fluids have been investigated extensively in vibration control (Stanway et al., 1996), seismic isolation (Makris et al., 1996), torque transmission (Choi and Lee, 2005), and so on. However, most of the previous studies merely considered the low-velocity and periodic movements, while very few investigations concerned about the dynamic response of the ER/MR devices under impact loadings.

Different from those in response to mechanical vibrations, the behaviors of ER dampers under impact loadings exhibit characteristics of high shear-rate, singe-stroke, large resistant force, and short duration. El-Wahed et al. (1999) studied the dynamic behaviors of MR and ER fluids in squeeze mode, but the effective energy absorbing stroke in this mode was very short and not suitable for impact energy absorbers. Lee et al. (2002) employed the Herschel-Bulkley model to analyze the dynamic response of the ER impact dampers, while Yeo et al. (2002) consider the response time and gave several numerical results for a semi-active ER damper. Song et al. (2002); Nam and Park (2007) studied ER and MR shock dampers under impulsive loadings, respectively. Batterbee et al. (2007a, 2007b) designed and investigated the response of MR landing gears. Although, the devices were designed for realistic impact velocities, experimental tests were performed at velocities below 0.5 m/s which were much lower than the real impact cases. On the other hand, Ahmadian and Norris (2004, 2008) conducted a series of impact tests by using two types of MR dampers with the maximum velocity as high as 7 m/s. From their experimental results, they found that the average crushing force of the MR dampers could be adjusted by the applied current. They also pointed out that the MR damper is controllable only when the impact velocity is lower than a

*Author to whom correspondence should be addressed. E-mail: metxyu@ust.hk
Figures 2–12, 15–17, A2 and A4 appear in color online: http://jim.sagepub.com

1045-389X/10/00 0001–17 $10.00/0 DOI: 10.1177/1045389X10366316

certain value because of high Reynolds Number. Although their conclusion seems partly reasonable, the definition of critical Reynolds number of non-Newtonian fluids is doubtful. According to Nouar and Frigaard (2001), the critical Reynolds Number depends on the Bingham Number, while in some previous papers (Ahmadian and Norris, 2008; Batterbee et al., 2007a), they assumed the critical Reynolds Number as 2000 or 1000. However, this problem is still unclear.

In this article, to study the performance of ER fluids in impact scenarios, the characterization of ER fluids flowing in parallel duct under high shear rate is first discussed. Both a nominal and exact characterization methods are evaluated and compared. Then, two types of ER fluids were experimentally characterized by means of a capillary rheometer with rectangular ducts, and their nominal yield stresses and viscosities under different electric fields determined. Afterwards, a double-ended ER cylinder with two parallel annular ducts was designed, and its dynamic responses to a mass impact under different electric field intensity and impact velocity were tested. Based on the experimental observations, the dynamic response of the ER cylinder was analyzed and a theoretical model proposed, in which the initial yielding, the inertia effect, and the response time of the ER fluid are mainly considered. Finally, the theoretical predictions of the dynamic response are compared with the experimental results, and the controllability of the ER cylinder is discussed.

CHARACTERIZATION OF ER FLUIDS UNDER HIGH SHEAR RATE

According to the previous study (Stanway et al., 1996), when subjected to high intensity electric field, the flowing behaviors of ER fluid can be approximated to be Bingham-plastic, whose constitutive equation is as follows:

$$\tau = \tau_0 + \mu\dot{\gamma} \tag{1}$$

where τ is the shear stress, $\dot{\gamma}$ is the shear rate, μ is the viscosity, and τ_0 denotes the yield stress of the ER fluid. Usually, it is assumed that τ_0 and μ are functions of the electric field intensity which is denoted by E (kv/mm). For theoretical modeling, most of the researchers employ the ideal yield stress and viscosity to evaluate the performance of ER fluid devices. However, in the experimental characterizations (Park et al., 1999; Chen and Wei, 2006; Goncalves et al., 2006) only the nominal yield stress and viscosity are measured by rheometers through the similar method as that for Newtonian fluids. Although, Choi et al. (2005) analytically evaluated the errors of rheological properties of ER fluid calculated from three different property models for both rotational co-axial cylinder and parallel-disk rheometers, there is still a lack of detailed analysis of capillary rheometer, which is suitable for high shear rate flowing.

Consider a capillary rheometer with a rectangular ER duct as illustrated in Figure 1(a) which has length L and width b, and the distance between the electrodes is h. If b is quite larger than h (e.g., $b \approx 10\,h$), the boundary effect at the narrow side can be ignored and the flow in the duct can be assumed as to be 1D flow. For the quasi-steady flow of ER fluids through the parallel duct, when it is free of electric field, the flowing behavior of the ER fluid is close to Newtonian and the contour of the stream lines has a parabola shape S1 as shown in Figure 1(b). After an electric field is applied, the stream lines change from S1 to S2. For the case S2, the ER fluid in the region between A and B does not yield and its shear rate is zero, but in the region between A, B, and the boundaries, the ER fluid yields. For ideal Bingham plastic flow, the analytical relation between the flow rate Q and the pressure drop ΔP through this duct can be obtained from (Stanway et al., 1996):

$$\Delta P^3 - \left(3\tau_0\frac{L}{h} + \frac{12\mu LQ}{bh^3}\right)\Delta P^2 + 4\tau_0^3\left(\frac{L}{h}\right)^3 = 0 \tag{2}$$

If the viscosity of the Bingham plastic fluid is known, for specified flow rate Q and pressure drop ΔP, the yield stress τ_0 can be obtained by the above equation. In most of the previously published papers about the characterization of ER/MR fluids, either Equation (2) was used to calculate the yield stress by assuming the viscosity to

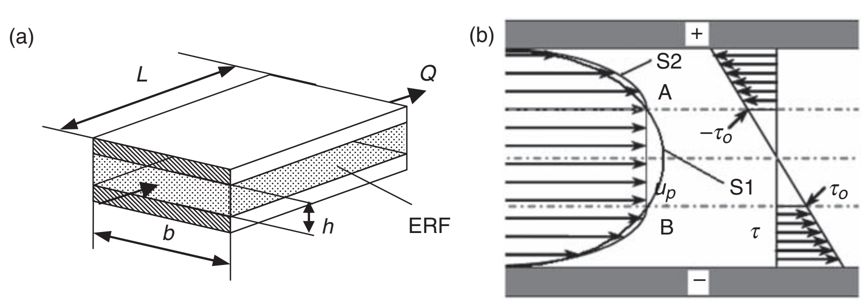

Figure 1. *The flowing behavior of ER fluid in parallel duct: (a) configuration of the ER duct; (b) cross-section of the duct.*

be constant (Lee and Choi, 2002; Goncalves et al., 2006) or similar method with Newtonian fluids was applied to calculate the shear rate and shear stress (Chen and Wei, 2006). However, for a new ER fluid whose yield stress and viscosity both need to be determined, Equation (2) alone is not sufficient. In the characterization tests, the flow of the fluid within the duct is quasi-steady, the shear stress along the boundary can be calculated by:

$$\tau_w = \Delta P \times \frac{h}{2L}. \tag{3}$$

If the stream-lines are assumed to be similar to those in a Newtonian flow, the nominal shear rate at the boundary of the ERF duct can be found as:

$$\dot{\gamma}_n = \frac{6Q}{bh^2}. \tag{4}$$

Hence, by employing Equations (3) and (4), the nominal flow curves of the ER fluid under different electric fields can be obtained. However, it should be noted that this method can only obtain exact shear stress and shear rate for Newtonian fluids. To obtain the true yield stress and viscosity of Bingham-plastic fluids, a similar method with Rabinowitsch's correction (Ferguson and Kembłowski, 1991) should be used.

Recalling to Equations (1) and (3), the true shear rate at the boundary should be:

$$\dot{\gamma}_w = \frac{\tau_w - \tau_0}{\mu} = -\frac{p}{\mu} \times \frac{h}{2} + \frac{\tau_0}{\mu}, \tag{5}$$

where $p = \Delta P/L$ is the pressure drop within a unit length of an ER duct. By taking the derivative of the both sides of Equation (2) and combining it with Equations (3) and (5), the true shear rate is found to be:

$$\dot{\gamma}_w = \frac{4Q}{bh^2} + \frac{2p}{bh^2} \times \frac{dQ}{dp}. \tag{6}$$

In the characterization tests, if the relationship between Q and p under a certain electric field is measured, by using Equations (3) and (6), the flow curve of this ER fluid can be calculated. As a result, the true yield stress and viscosity of the ER fluid can be obtained by fitting the data. Compared with the previous nominal characterization method, this method is denoted as exact characterization method in the subsequent text.

In order to verify the above exact characterization method and evaluate the errors of the nominal method, a numerical validation procedure is proposed as follows. First, for this rheometer, take the same set of the geometric parameters as those adopted by Zhang et al. (2008); that is, the width and the gap of the ER duct are $b = 10$ mm and $h = 1.2$ mm, respectively; and the

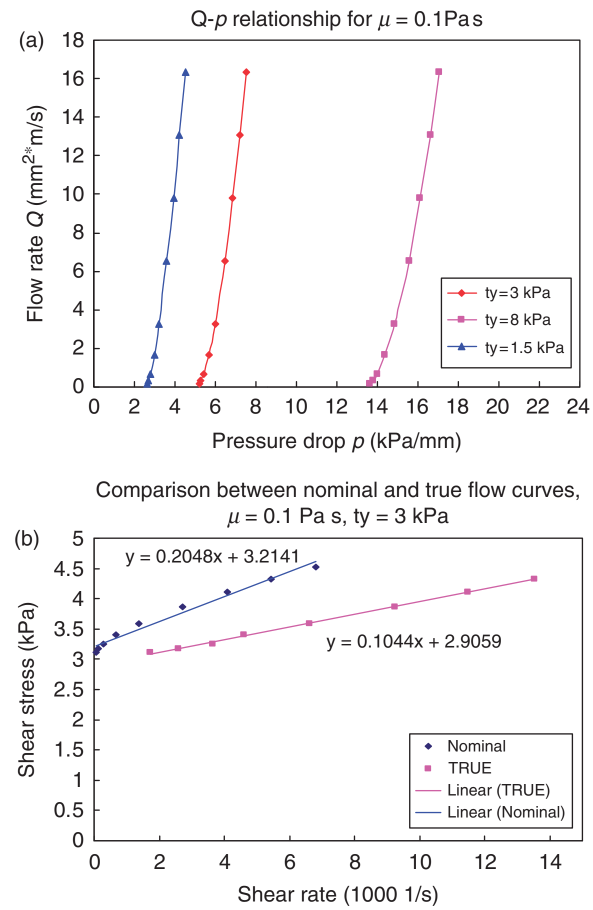

Figure 2. *Numerical comparison between two characterization methods: (a) typical relations between Q and p; (b) comparison between the nominal and exact characterization methods for ERF with $\mu = 0.$ Pa s and $\tau_0 = 3$ kPa.*

piston area is $A_p = 1963$ mm^2. Then, assume the ER fluids are ideal Bingham plastic fluids, and different rheological properties are evaluated, which are $\mu = 0.1$, 0.5, 1.5 Pa s and $\tau_0 = 1.5$, 3.0, and 8.0 kPa; choose a group of piston velocities as $V_p = 10$, 50, 100, 200, 300, 400, and 500 mm/min. For a certain combination of μ and τ_0, the relationship between flow rate Q and pressure drop p can be obtained by means of Equation (2); according to the true Q-p relations, both the nominal and exact characterization methods are employed to calculate the shear rate-stress curves. Finally, by the linear fitting of these flow curves, the nominal and true rheological properties are obtained and compared with the theoretical values.

Figure 2(a) illustrates the results of the relationships between Q and p for $\mu = 0.1$ Pa s and $\tau_0 = 1.5$, 3.0, 8.0 KPa. It is seen that when the flow rate Q is small, the Q–p curve is non-linear. However, when Q becomes very large, the Q–p curves approach to linear relations. Figure 2(b) depicts the comparison of the two characterizations for $\mu = 0.1$ Pas and $\tau_0 = 3$ KPa, showing that with the same flowing conditions, the shear rate measured by the exact method is much larger than that by

Table 1. Comparison between the nominal and exact characterization methods.

		Nominal μ (Pa s)	True μ (Pa s)	Nominal τ_0 (kPa)	True τ_0 (kPa)
$\mu = 0.1$ Pa s	$\tau_0 = 1.5$ KPa	0.163 (63%)	0.104 (4%)	1.65 (10%)	1.4 (6.7%)
	$\tau_0 = 3.0$ KPa	0.205 (105%)	0.104 (4%)	3.21 (7%)	2.91 (3%)
	$\tau_0 = 8.0$ KPa	0.299 (200%)	0.104 (4%)	8.35 (4.4%)	7.84 (2%)
$\tau_0 = 3$ KPa	$\mu = 0.1$ Pa s	0.205 (105%)	0.104 (4%)	3.21 (7%)	2.91 (3%)
	$\mu = 0.5$ Pa s	0.64 (28%)	0.52 (4%)	3.45 (15%)	2.83 (5.7%)
	$\mu = 1.5$ Pa s	1.64 (9.3%)	1.53 (2%)	3.70 (23%)	2.80 (6.7%)

Note: The percentages in the brackets are the errors compared with the theoretical values.

the nominal one. Compared with the theoretical values, while the yield stress obtained by the nominal method is acceptable, the nominal viscosity has an error more than 100%. On the other hand, the exact characterization method can achieve very good agreement with the theoretical values.

More numerical characterization examples are listed in Table 1, which demonstrates that for the given rheological properties, by using the exact characterization method, the errors in the viscosity is always smaller than 5%, while the errors in the yield stress is smaller than 7%. However, the errors of nominal properties are very large. The results also show that with the same viscosity, the errors in the nominal viscosity increases with the increase of yield stress, whilst the error in the nominal yield stress decreases. Similar observations are made when the yield stress remains unchanged.

For ideal Bingham-plastic fluids, if Equation (2) is non-dimensionalized by τ_0/h, the non-dimensional flow rate and pressure drop are as follows:

$$\bar{q} = \frac{12\mu Q}{bh^3} \times \frac{1}{(\tau_0/h)}, \quad \bar{p} = \frac{p}{\tau_0/h}, \tag{7}$$

Then, Equation (2) can be rewritten as:

$$\bar{p}^3 - (3 + \bar{q}) \cdot \bar{p}^2 + 4 = 0 \tag{8}$$

The relationship between $\bar{p}$ and $\bar{q}$ for $\bar{q}$ from 0 to 10 are plotted in Figure 3(a), which indicates that when the flow rate Q approaches to 0 and infinite, the relationship between Q and p can be approximated by a liner relationships as follows:

$$Q \to 0, \quad p \to \frac{12\mu Q}{bh^3} + \frac{2\tau_0}{h}, \tag{9}$$

$$Q \to \infty, \quad p \to \frac{12\mu Q}{bh^3} + \frac{3\tau_0}{h}. \tag{10}$$

Therefore, for any flow conditions, we have:

$$p = \frac{12\mu Q}{bh^3} + K \cdot \frac{\tau_0}{h}, \text{ where } 2 < K < 3. \tag{11}$$

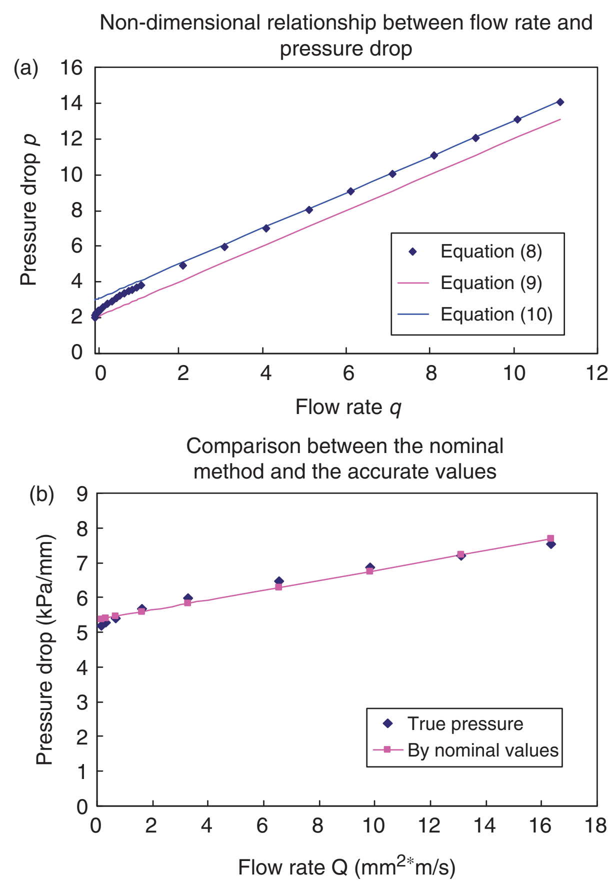

Figure 3. *Analysis of the nominal characterization method: (a) relationship between non-dimensional flow rate and pressure drop; (b) error evaluation of the pressure drop from nominal rheological properties.*

Recalling Equation (5), it is found that when $K = 2$, Equation (11) becomes Equation (4), which means that the nominal method is corresponding to Equation (11) with $K = 2$, i.e., Equation (9). To make use of the nominal rheological properties, for given flow rate Q, Equation (9) is used to calculate the pressure drop and the results are compared with the values obtained from true yield stress and viscosity and the non-linear Equation (2). It can be seen from Figure 3 that by using the nominal rheological properties, the pressure drop obtained by the linear Equation (9) can achieve

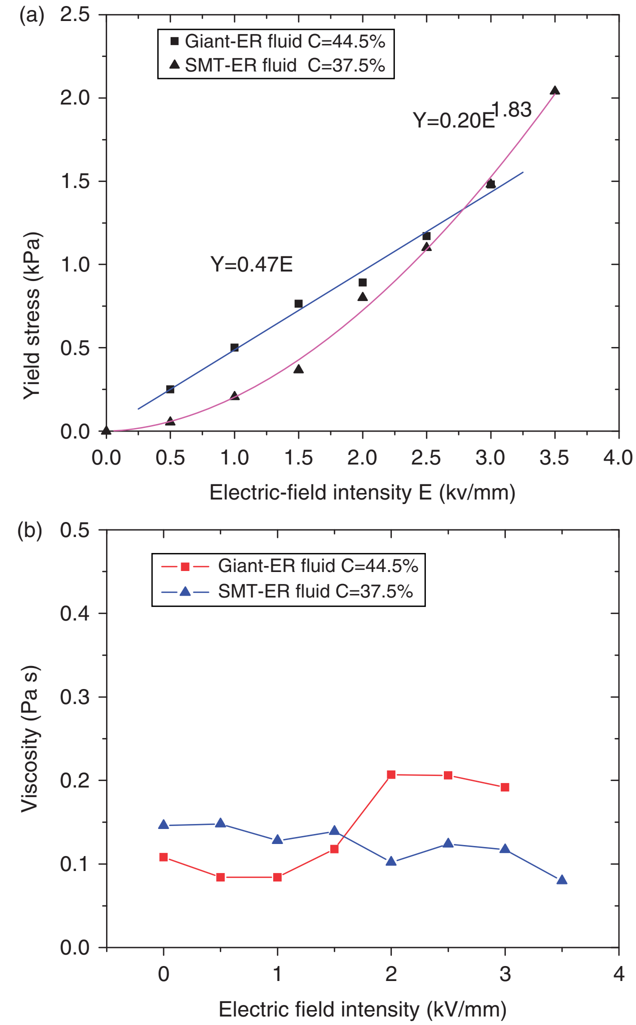

Figure 4. *(a) The nominal yield stresses of the ER fluids; (b) nominal viscosity of the ER fluids.*

very good agreement with the real values. Therefore, although the nominal characterization method can not obtain the real rheological properties, in the theoretical modeling of ER fluid flows, the nominal properties are still useful and can greatly simplify the calculation of the pressure drop.

For the experimental study of the ER impact energy absorber, two kinds of ER fluids are employed. The first one is labeled by Giant-ER fluid, which was produced in the HKUST by dispersing nano-particle coated $Ba_{0.8}(Rb)_{0.4}TiO(C_2O_4)_2$ particles in silicon oil (Wen et al., 2004). The mass concentration of the particles is $C = 44.5\%$. The other ER fluid named as SMT-ER fluid was purchased from Smart Technology Limited and labeled by LID3354S, which is density-matched and has a mass concentration $C = 37.5\%$. After characterization by means of the capillary rheometer (Zhang et al., 2008), the nominal yield stress and viscosity of these two ER fluids with respect to different electric field intensity are plotted in Figure 4(a) and (b), respectively. In the subsequent experiments and modeling, these rheological properties will be used.

DESIGN OF THE ER FLUID IMPACT ENERGY ABSORBER

Up to now, two typical designs for ER cylinders have been reported in literature (Ahmadian and Norris, 2008), which are single-ended and double-ended, respectively. The former is compact in structure, but requires a chamber filled with high pressure gas, which makes it complicated, while the double-ended design is relatively simple in design and implementation. Hence, in this article, for simplicity, the double-ended design is chosen.

Considering that the density and plastic viscosity of our ER fluids are about $\mu = 0.15\,\text{Pas}$ and $\rho = 1.0 \times 10^3\,\text{kg/m}^3$, and their maximum mean flow speeds in the duct are lower than 10 m/s, the Reynolds number, $R_e = \rho v Q/\mu b$, (Batterbee et al., 2007), will be lower than 200. Therefore, the flow can be assumed to be laminar. If ignoring the influences of the compressibility and inertia effect of the ER fluid, the resistant force of a typical ER fluid cylinder can be approximated by:

$$F_d = \left(\frac{12\mu_n Q}{bh^3} + 2 \cdot \frac{\tau_{0-n}}{h}\right) \cdot L \cdot A_p + F_R, \qquad (12)$$

where the μ_n and τ_{0-n} are the nominal viscosity and yield stress of the ER fluid, and F_R is the friction force. In the subsequent sections, μ_n and τ_{0-n} will be replaced by μ and τ_0 for convenience. The first and second terms in the bracket on the right-hand side of Equation (12) are the contributions of viscosity and yield stress, which will be termed as the viscous and ER effects, respectively. For impact scenarios, since the shear rate is high, to reduce the viscous effect and increase the controllability of the ER fluid cylinder, the width b of ER duct should be as large as possible. Accordingly, a double-ended ER cylinder with two parallel annular ducts was designed, whose cross-section along its axis is as shown in Figure 5(a). This ER cylinder is mainly composed of three coaxial cylindrical tubes sealed by insulated plates at their two ends. The gaps between the neighboring tubes form the ER ducts. During the tests, inner-most and outer tubes are connected to the ground (negative electrode), while the middle tube is connected to the positive electrode. When the piston rod moves downwards, the ER fluid in the lower chamber will be forced to move down and go back to the upper chamber through the ER ducts. By adjusting the electric field applied to the ER ducts, the flow behaviors of the ER fluid as well as the resistant force of the rod can be controlled. The important dimensions of the ER cylinder are depicted in Figure 5, in which the gap and the effective length of the duct are

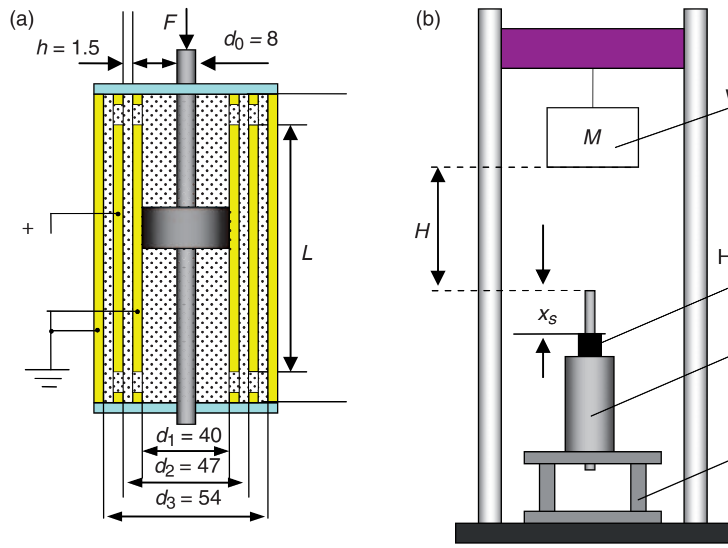

Figure 5. *(a) Cross-section of the ER cylinder; (b) schematic diagram of the experimental setup.*

$h = 1.5$ mm and $L = 65$ mm, respectively. Therefore, the effective cross-sectional areas of the piston and the ducts, the width of ER duct are as follows:

$$A_p = \frac{\pi}{4} \times \left(d_1^2 - d_0^2\right) = 1206.4\,\text{mm}^2, \tag{13}$$

$$A_d = \frac{\pi}{4}\left[d_2^2 - (d_2 - 2h)^2 + d_3^2 - (d_3 - 2h)^2\right]$$
$$= 461.8\,\text{mm}^2 \quad \text{and} \quad b = \frac{A_d}{h} = 308\,\text{mm}. \tag{14}$$

If assuming the ER fluids in the two channels have the same velocity, then the velocity ratio between the piston and the ER fluid inside the ducts is:

$$R_s = \frac{A_p}{A_d} = 2.61 \tag{15}$$

In our experimental study, the two types of ER fluids mentioned in the previous section were filled into the ER cylinder and tested, respectively. A Dynatup 8250 Drop-weight Tester was used for the impact tests and a diagram of the testing system is shown in Figure 5(b). The ER cylinder and its supporting platform were placed at the bottom of the Drop-weight Tester, while a weight with mass M was employed to impinge the piston rod of the ER cylinder. Before the impact test, the piston rod was first pulled to its top limited location and an electric field was applied, then the weight dropped down from height H and impinged the piston rod connected to the ER cylinder. The loading history was recorded by the load cell. In order to avoid excessive shock and protect the devices, a piece of rubber was placed between the crosshead and the piston rod, and a honeycomb block was also employed as shown in Figure 5(b). The total drop mass including the weight, the load cell, and the crosshead in this test was $M = 5.67$ kg.

EXPERIMENTAL RESULTS

Quasi-steady Tests

The ER cylinder was first compressed quasi-steadily with a loading speed 40 mm/min on the UTM SINTECH 10/D installed at HKUST. During the experiments, the UTM was first turned on to let the crosshead compress the piston rod of the ER cylinder, and then the electric field was applied to the ER duct when the displacement was about 5 mm. This procedure can avoid the damage of the device, because the static yield stress of the ER fluid may be very large so that the ER duct may get completely jammed. Considering the amplifying ratio of the ER fluid velocity was $R_s = 2.61$ and the loading speed of the machine was 40 mm/min, the real flow speed of the ER fluids inside the channel would be $V_d = 1.93$ mm/s. By using Equation (12), it is found that the viscous force is lower than 0.5 N. Hence, in the quasi-steady tests the viscous force can be ignored compared with the ER force.

Figure 6(a) shows the quasi-steady loading curves of the ER cylinder filled with Giant-ER fluid under different electric field intensities. It can be seen that even when the electric field intensity is zero (i.e., $E = 0$ kv/mm), there is still a resistant force $F_R \approx 100$ N. Since at this loading speed, the viscous and ER forces are both negligible, this resistant force is attributed to the friction between the piston rod and the inner wall of the tube. With the increase of E, the resistant force increases, too. However, the fluctuation of the force is very obvious, because the real flow inside the ER duct is not

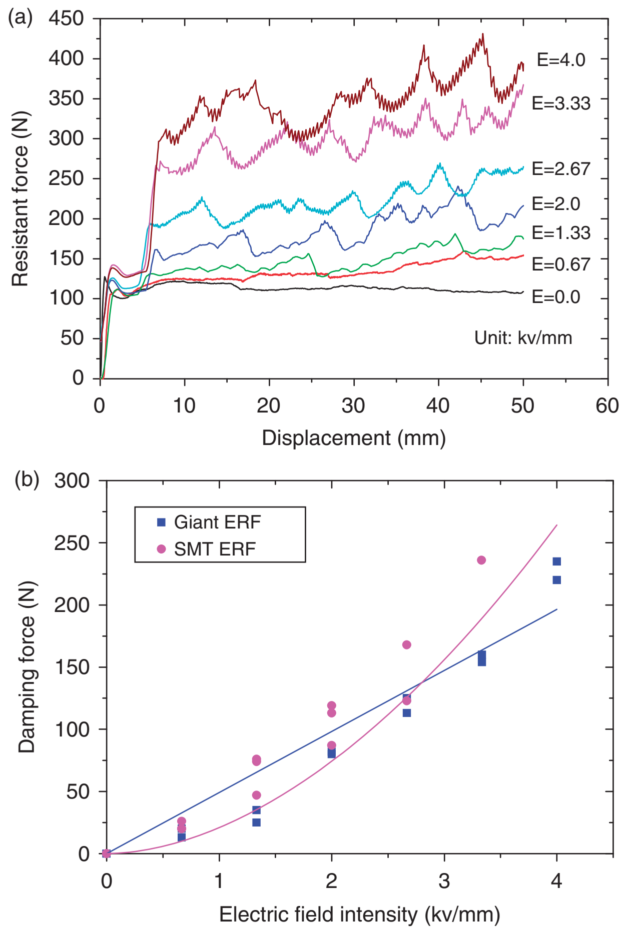

Figure 6. *(a) Loading curves for Giant-ER fluid under different electric fields; (b) comparison between experimental resistant forces and those predicted by the material properties.*

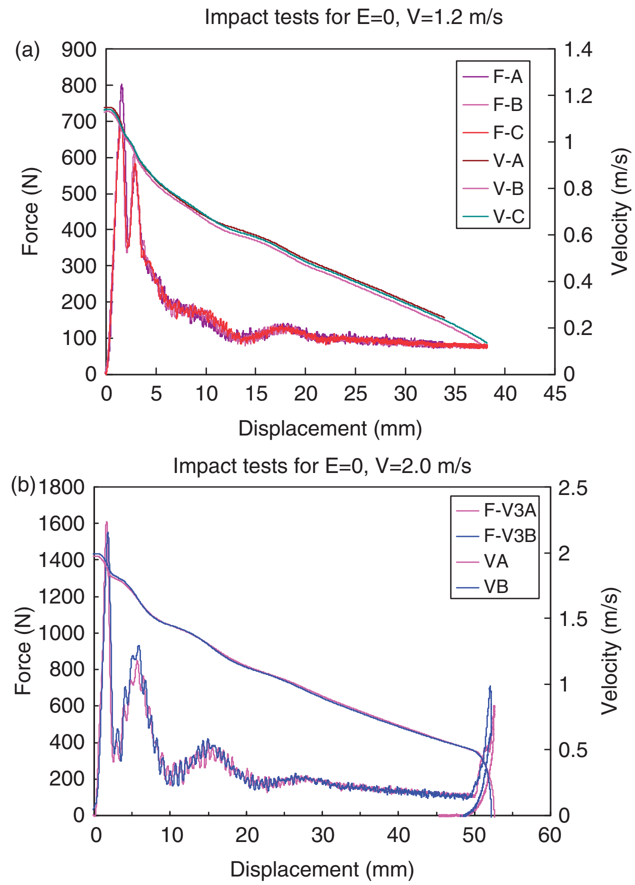

Figure 7. *Typical loading and velocity histories for the impact tests with $V_0 = 1$ and 2 m/s.*

continuous, which was observed during the characterization tests (Zhang et al., 2008). When $E = 4.0$ kv/mm, the average resistant force of the ER cylinder is about 350 N. On the other hand, the friction force of SMT-ER fluid is 80 N and the maximum electric field intensity is 3.5 kv/mm. It should be noted that in the experiments, the particles of ER fluids were very coarse and the lubricant of the ER cylinder was not satisfactory.

After subtracting the friction force, the experimental resistant forces with respect to the electric field for the ER cylinders filled with Giant-ER and SMT-ER fluids are depicted in Figure 6(b). For comparison, the resistant forces predicted by Equation (12) are also plotted. It is revealed that although the dispersion of the experimental results is relatively large, the accuracy of the results is acceptable within this range of electric field intensity.

Impact Tests of the ER Cylinders

The impact tests were conducted on a Dynatup-8250 testing machine as shown in Figure 5(b). For each type of ER fluids, except the case with $E = 0$, four other electric field intensities from 1.33 to 3.33 kv/mm were applied to the ER duct, and for every intensity, three impact velocities, about 1.2 m/s, 2.0 m/s, and 3.0 m/s, were tested. Two typical loading and velocity histories for the impact tests of the ER cylinder filled with Giant-ER fluid under $E = 0$ are plotted in Figure 7(a) and (b), in which the impact velocities are about 1.2 and 2.0 m/s, respectively. For each impact condition, two or three repeat tests were conducted, which were denoted by A, B, and C. The results confirmed that the repeatability of the tests was good. A typical loading curve of this dynamic response possesses an initial peak force followed by some fluctuations, and then the force gradually decreases. After a certain displacement, the decrease of the resistant force becomes very slow. The initial peak force for the two impact conditions is about $F_{\text{peak}} = 800$ N and 1600 N, respectively. It should be noted that for the impact velocity of about $V_0 = 2$ m/s, the effective energy absorbing stroke was finished at the displacement $x_s = 50$ mm. However, at this moment, the weight still had a velocity of about 0.5 m/s and the crosshead was finally stopped by the honeycomb as shown in Figure 5(b). Consequently, when the displacement

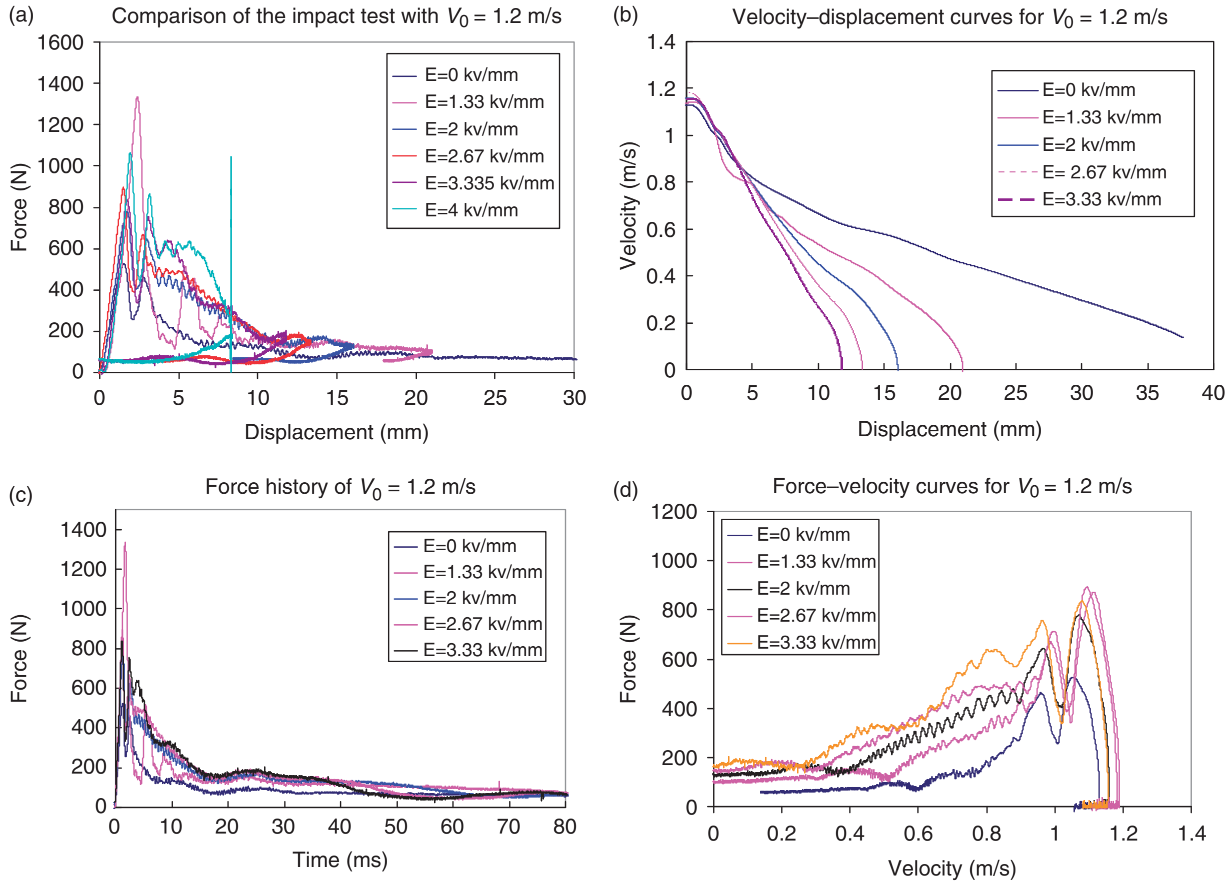

Figure 8. *The test results for the ER cylinder filled with Giant-ER fluid under $V_0 = 1.2$ m/s: (a) F–x; (b) V–x; (c) F–s; (d) F–V.*

exceeded 50 mm, the load increased greatly whilst the velocity was soon reduced to zero.

Figure 8 exhibits the experimental results for the ER cylinder filled with Giant-ER fluid under impact velocity $V_0 = 1.2$ m/s and different electric fields. It is seen from Figure 8(a) that the configurations of the load-displacement curves are similar to those with $E = 0$, and higher the electric field intensity, the larger the resistant force. Also, it is revealed by Figure 8(b) that in the initial impact stage, the decrease of the velocity is faster than that in the subsequent stage and the final displacement decreases with the increase of the electric field intensity. The curves of the load history are plotted in Figure 8(c), which indicate that most of the impacts lasted no more than 50 ms.

However, it is difficult to fully explore the effect of the electric field simply by comparing the loading and velocity histories, because the resultant force always contains both the viscous and ER effects. To decouple these two effects, the force-velocity curves are re-plotted in Figure 8(d). With the initial velocity of this test $V_0 = 1.2$ m/s, the curves in Figure 8(d) should be read from right to left and the difference between the resistant forces under the same velocity represents the ER effect. It also reveals that the entire impact process has three distinct stages. In the first stage, there is an initial peak, after which the load fluctuates, and then decreases gradually. In the second stage, the effect of the electric field is quite prominent. After a transition between the second and the third impact stages, the loading curve becomes smooth.

The test results for this ER cylinder under the impact velocity $V_0 = 3$ m/s are also illustrated in Figures 9(a)–(d). Compared with the results for $V_0 = 1.2$ m/s, the initial peaks under $V_0 = 3$ m/s are much higher. At the end of the energy absorbing stroke of 50 mm, the initial kinetic energy in some cases has not been fully absorbed by the ER cylinder. As a result, the residual energy has to be dissipated by the honeycomb block. From the load history curves, the difference between the cases with different E is very small. However, in Figure 9(b), at the displacement 50 mm, the residual velocity under more intense electric field is larger than that under weaker electric field. Also, the duration of the impact response is about 30–40 ms, which is shorter than that in the case of $V_0 = 1.2$ m/s. Figure 9(d) shows that under high impact velocity, the ER effect in the second stage seems to be very small, while that

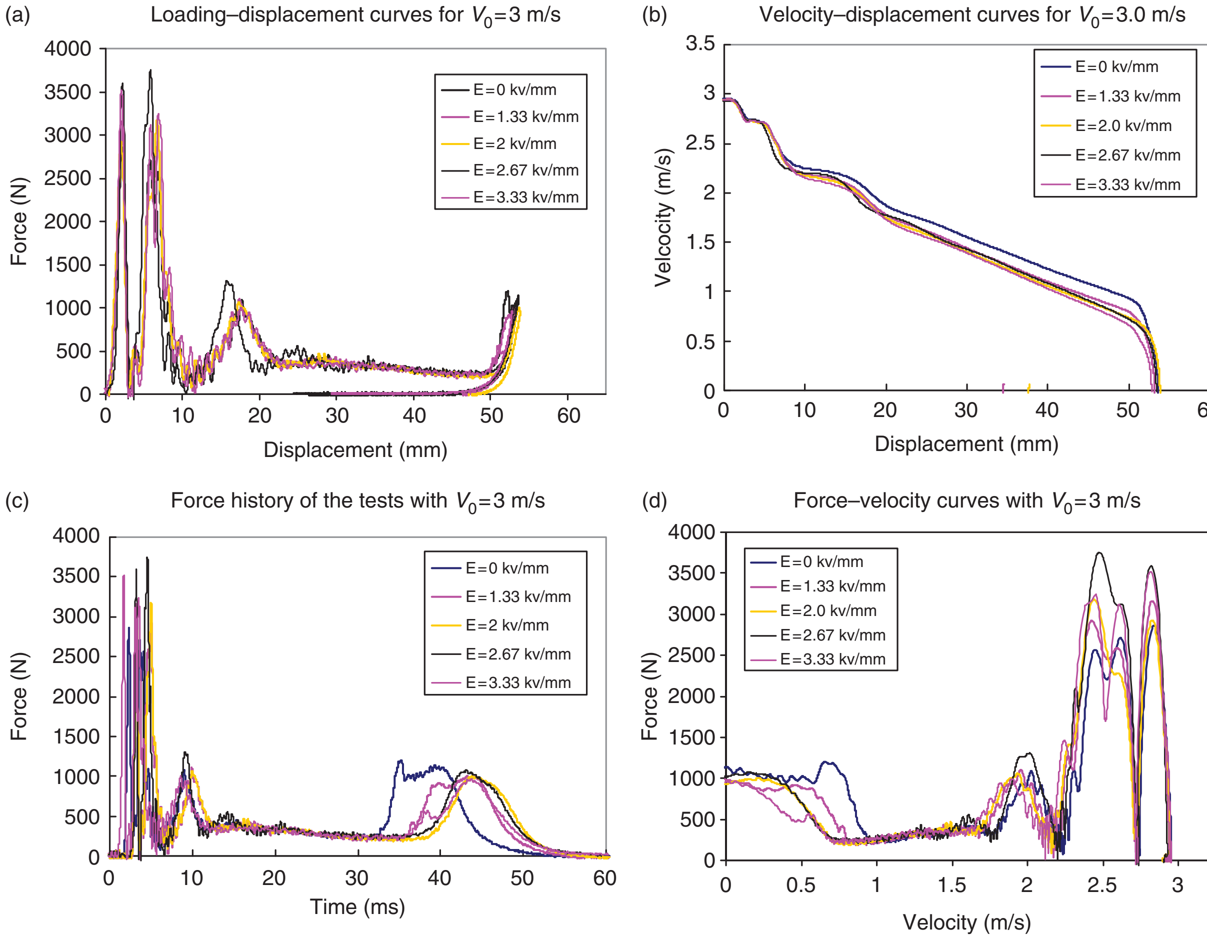

Figure 9. *The test result for the ER cylinder filled with Giant-ER fluid under $V_0 = 3$ m/s: (a) F–x; (b) V–x; (c) F–s; (d) F–V.*

in the third stage it almost disappears. Therefore, compared with the test under $V_0 = 1.2$ m/s, the ER effect under 3 m/s becomes weaker.

In addition, the impact tests for the ER cylinder filled with SMT-ER fluid were also conducted, and the initial peak forces for the cylinders filled with the two ER fluids (Giant-ER and SMT ER fluids) under different impact velocities are plotted in Figure 10(a) and (b). It can be seen that, although the electric field intensity has certain influence on the peak force, the dominant factor is the impact velocity; and with the increase of the impact velocity, the initial peak force increases greatly.

The mean crushing forces during the impact tests are also calculated based on the experimental results. The calculation method is as follows:

$$F_m = \begin{cases} \dfrac{\frac{1}{2} M \times V_0^2}{x_f}, & x_f < x_s \\ \dfrac{\frac{1}{2} M\left(V_0^2 - V_s^2\right)}{x_s}, & x_f > x_s \end{cases} \tag{16}$$

where x_f is the final displacement of the piston, x_s is the limit of the energy absorbing stroke (i.e., displacement of the piston when the impinger contacted the honeycomb block, which was set to be 50 mm) and V_s is the residual velocity of the piston at $x = x_s$. The results of mean forces for the ER cylinder filled with the two ER fluids are depicted in Figure 11(a) and (b), respectively. In these figures, the results for $V_0 = 0$ m/s are from the quasi-steady compression tests. It is shown that with the increase of electric field intensity, the mean crushing force increases. However, for larger impact velocity this ER effect becomes weaker. As shown in Figure 11(a), under $V_0 = 3$ m/s the mean crushing force of cylinder with Giant-ER fluid nearly has no increase, even when E increases from 0 to 4 kv/mm. On the other hand, although the F_{m} for SMT-ER fluid has a slight increase, the enhancement due to electric field under higher velocity is weaker than that under smaller velocity.

THEORETICAL MODELING FOR THE IMPACT RESPONSE OF ER CYLINDER

Based on the experimental observations as shown in Figures 8 and 9, it is found that an entire impact response of the ER cylinder consists of three distinct

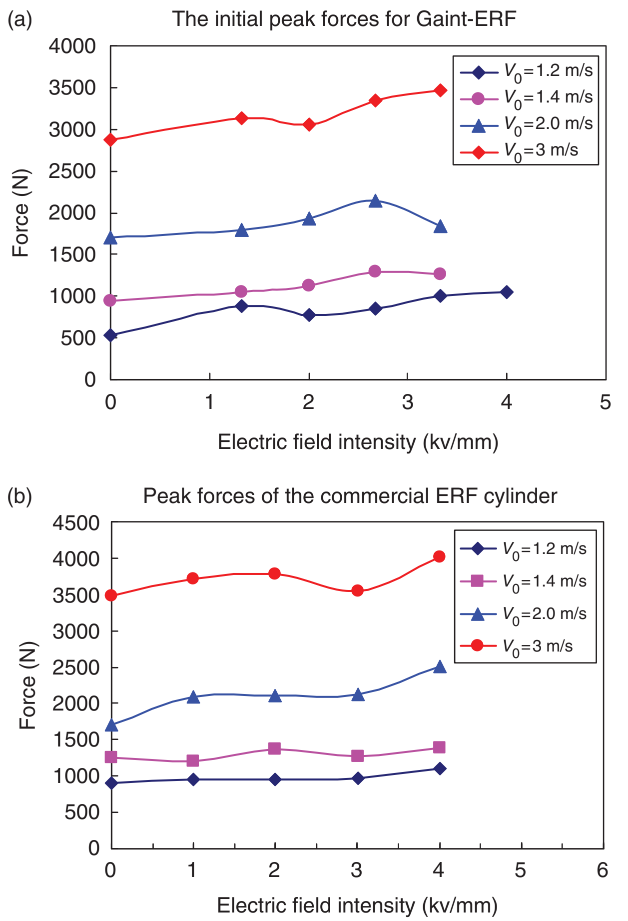

Figure 10. *Peak forces of the ER cylinders under different impact conditions: (a) filled with Giant-ER fluid; (b) filled with SMT-ER fluid.*

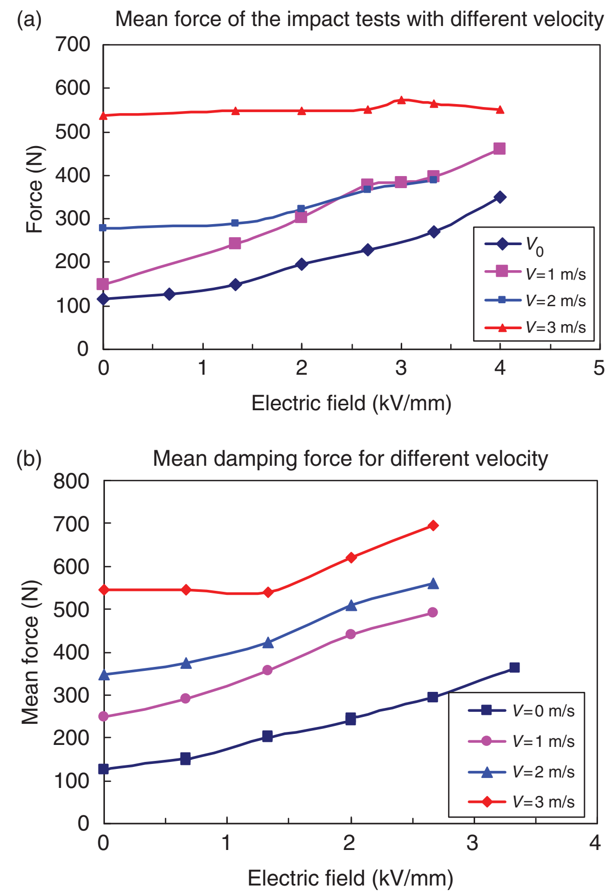

Figure 11. *Mean crushing force of the ER cylinders: (a) filled with Giant-ER fluid; (b) filled with SMT-ER fluid.*

stages, namely, the initial shock stage, a transition stage, and a smooth flow stage. In this section, the initial shock and the subsequent two stages will be analyzed step by step.

Modeling of the Initial Shock Stage

The initial shock stage is characterized by a peak force followed by some fluctuations. Before the impact, the impinger has a velocity V_0, while the piston rod is stationary; after they contact each other, the impinger decelerates and the piston rod accelerates until they gain the same velocity. To avoid a rigid-to-rigid impact, a rubber plate of thickness 4 mm was placed between the impinger and the piston rod. As the fluctuations are caused by the wave propagation and vibration of the set-up, rather than the dynamic behavior of the ER cylinder, these effects are ignored in the modeling analysis. Besides, according to the preliminary analysis as shown in the Appendix, the compressibility of the ER fluid only affects the initial impact stage, while the inertial effect functions through the entire process, especially when the density of the fluid is large (e.g., MR fluids). Therefore, the influences of the four factors, that is, the compression of the rubber, the initial yielding, compressibility, and the inertial effect of the ER fluid, will be investigated in this section.

The proposed theoretical model is sketched in Figure 12(a), in which X_1 and X_2 are the displacements of the crosshead and the piston rod, respectively, while the governing equations of the system are given by:

$$M\ddot{X}_1 = Mg - F_k, \tag{17a}$$

$$m\ddot{X}_2 = mg + F_k - F_d, \tag{17b}$$

where M denotes the mass of the weight together with the load cell and crosshead, m is the mass of the piston and ER fluid, F_k is the compressive force of the rubber plate and F_d is the resistant force of the ER cylinder.

To determine F_k, a quasi-static compression test for the rubber plate was conducted, in which the contact conditions were kept the same as those in the impact tests. The result is plotted in Figure 12(b), showing that its load–displacement relationship can be approximated by:

$$F_k = 1068\Delta - 1311\Delta^2 + 656\Delta^3, \text{ where } \Delta = X_1 - X_2. \tag{18}$$

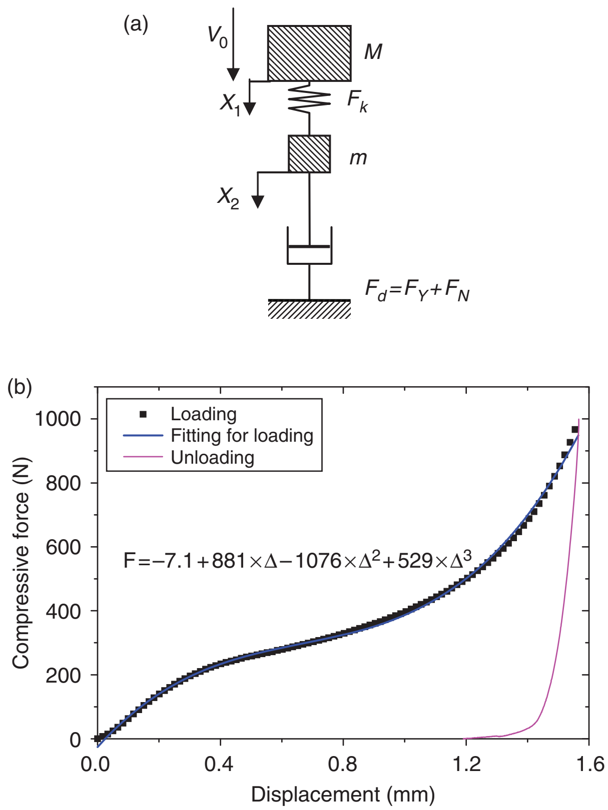

Figure 12. (a) Analytical model for the initial shock stage; (b) compression curve for the rubber plate.

In the unloading process, the compressive force drops sharply and the deformation of the rubber is irrecoverable. Although the dynamic properties of the rubber plate may have some differences between the quasi-static results, it will not influence the dynamic response very much.

Relevant to the resistant force F_d, it is mainly contributed by the viscous and ER effects of the ER fluid. Two different types of yield stresses for the ER fluid, i.e., the quasi-static yield stress τ_{YS} and the dynamic yield stress τ_{YD} $(=\tau_0)$, should be distinguished. Before starting to flow, the ER fluid has to overcome the quasi-static yield stress and its deformation tends to be viscous-elastic. The constitutive relation of the ER fluid can be expressed by:

$$\tau = \begin{cases} G\gamma + \mu\dot{\gamma}, & \gamma < \gamma_S \\ \tau_0 + \mu\dot{\gamma}, & \gamma > \gamma_S \end{cases}, \tag{19}$$

where G is the shear modulus of the ER fluid before yielding and $\gamma_S = \tau_{YS}/G$ is the yield shear strain. On the other hand, recalling the Equations (A1) and (A4) for the fluid compressibility, the flow rate Q is:

$$Q = A_p\left[\dot{X}_2 - \frac{(L - X_2)}{\beta}\dot{P}\right], \tag{20}$$

where β is the bulk modulus of the ER fluid.

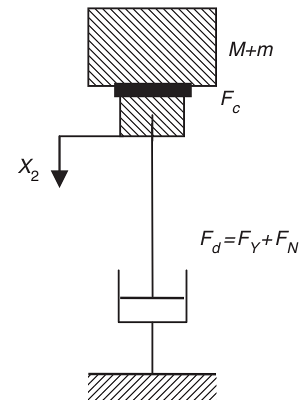

Figure 13. Analytical model for the second and third impact stages.

Besides, considering the inertia effect of the ER fluid in Equation (A9), and combining Equations (12) and (19), we have:

$$\begin{cases} \dot{X}_2 = 0, & (mg + F_k) < F_R \\ F_d = \left(\dfrac{12\mu Q}{bh^3} + 2\cdot\dfrac{G\gamma}{h} + \rho\dfrac{A_p}{bh}\cdot\overset{\mp}{\ddot{X}_2}\right)\cdot L\cdot A_p + F_R, & \gamma < \gamma_S \\ F_d = \left(\dfrac{12\mu Q}{bh^3} + 2\cdot\dfrac{\tau_0}{h} + \rho\dfrac{A_p}{bh}\cdot\overset{\mp}{\ddot{X}_2}\right)\cdot L\cdot A_p + F_R, & \gamma > \gamma_S \end{cases} \tag{21}$$

At the end of the initial shock stage, the compression of the rubber plate has exceeded its elastic range. However, to simplify the model, the spring-back of the rubber plate is ignored, so that the weight and the piston rod will move together after they gain the same velocity at the end of the initial shock stage.

Analysis of the Second and Third Stages

In the second impact stage, the weight and the piston rod move together, so that the motion of the system is represented by Figure 13 and the governing equation becomes:

$$(M + m)\ddot{X}_2 = (M + m)g - F_d. \tag{22}$$

Because the compressibility of the ER fluid only affects the initial stage, in the second and third impact stages, it will be ignored, which means that Equation (20) becomes $Q = A_p\dot{X}_2$. Also, the inertia effect of ER fluid is still considered by Equation (21). However, since the duration of the impact process is of the same scale as the response time of the ER fluid to the applied electric field, the effect of this response time should be taken into account.

Different from the quasi-steady tests under low velocity, as shown in Figure 14(a), there are two types of ER

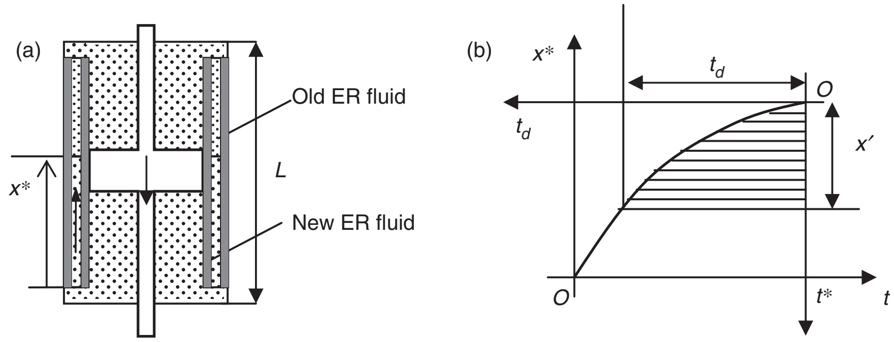

Figure 14. *(a) Status of the ERF inside the duct; (b) diagram for the calculation of dwell time.*

fluids inside the ducts, namely, the old ER fluid which has been in the duct before the impact, and the new ER fluid which just enters the ducts pushed by the piston. The yield stress of the old ER fluid under the electric field has been developed, but the yield stress of the new ER fluid has not been fully developed, because their dwell time under the electric field is too short. In the analysis of the previous stage, because the duration of the initial shock is small, the new ER fluid and the effect of the response time are negligible. However, when this new ER fluid section becomes longer, it should be considered. Assume the response time of the ER fluid to the applied electric field is t_R (which is usually 30–50 ms) and the yield stress increases linearly with the dwell time, then the instantaneous yield stress is:

$$\tau_Y = \tau_0 \times \min\left(\frac{t_d}{t_R}, 1\right) \tag{23}$$

where t_d is the dwell time of the ER fluid within the duct. As shown in Figure 14(a), it is assumed that at a certain moment t, the interface between the old and new ER fluids locates at x^*. A diagram relationship of $x^* - t$ is illustrated in Figure 14(b), which indicates that the dwell time t_d for any ER fluid at the position x' can be obtained from another coordinate system $x' - t_d$ by:

$$x' = \int_{t-t_d}^{t} \dot{x}\,\mathrm{d}t \quad \text{or} \quad t_d(x') = t(x^*) - t(x^* - x'), \tag{24}$$

where $x^* = R_s X_2$. Therefore, in Equation (21) the resistant force F_d in the second impact stage can be expressed as:

$$F_d = A_p\left[\Delta p_0(L - x^*) + \int_0^{x^*} \Delta p \mathrm{d}x + +\rho\frac{A_p}{bh}\cdot L \cdot \ddot{X}_2\right] + F_R, \tag{25}$$

where:

$$\Delta p_0 = \frac{12\mu Q}{bh^3} + \frac{2\tau_0}{h} \quad \text{and} \quad \Delta p = \frac{12\mu Q}{bh^3} + \frac{2\tau_0}{h}\min\left(\frac{t_d}{t_R}, 1\right). \tag{26}$$

When x^* is equal to L, all the old ER fluid has been pushed out of the duct, so the dynamic response enters the third impact stage, namely, the smooth flow stage, in which the resistant force becomes:

$$F_d = A_p \int_0^L \Delta p\,\mathrm{d}x + F_R, \tag{27}$$

where Δp is still defined by Equations (24)–(26).

In the second and third impact stages, the compressive force applied to the load-cell can be obtained from:

$$F_c = M(g - \ddot{X}_2) \tag{28}$$

For given initial conditions, the theoretical predictions of the dynamic response of the ER cylinder can be obtained by means of Runge–Kutta method.

Results for the Theoretical Modeling

To verify this model and investigate the influences of different parameters, the geometric conditions adopted in the experiments are used in theoretical calculation. On the other hand, the density and bulk modulus of the ER fluids are assumed to be $\rho = 1.0 \times 10^3\,\mathrm{kg/m^3}$ and $\beta = 1.0\,\mathrm{GPa}$. However, three unknown parameters G, γ_S, and t_R, have to be estimated. To evaluate the effects of these parameters, the yield stress of the ERF are assumed to be $\tau_{YS} = K_t\tau_{YD}$ and $\gamma_S = 2, 5, 10$, so G can be obtained by: $G = \tau_{YS}/\gamma_S$ accordingly. The shear rate and shear stain in the visco-plastic deformation stage of the ERF are approximated by Newtonian flow as governed by Equation (4).

A typical impact event with $V_0 = 2\,\mathrm{m/s}$, $M = 5.67\,\mathrm{kg}$, $m = 0.25\,\mathrm{kg}$, $\mu = 0.15\,\mathrm{Pa\,s}$, $\tau_{YD} = 1.5\,\mathrm{kPa}$, and $F_R = 100\,\mathrm{N}$ is first analyzed by this model. Figure 15(a) plots the predicted responses of the initial shock stage with $K_t = 1.5$, 3, 6, and $\gamma_S = 2$, 5, 10. It shows that the static yield stress influences the value of the initial peak forces, and the yield shear strain affects the displacement of the piston. It should be pointed out that since the energy dissipation during this stage is relatively small, these factors do not affect the subsequent two stages.

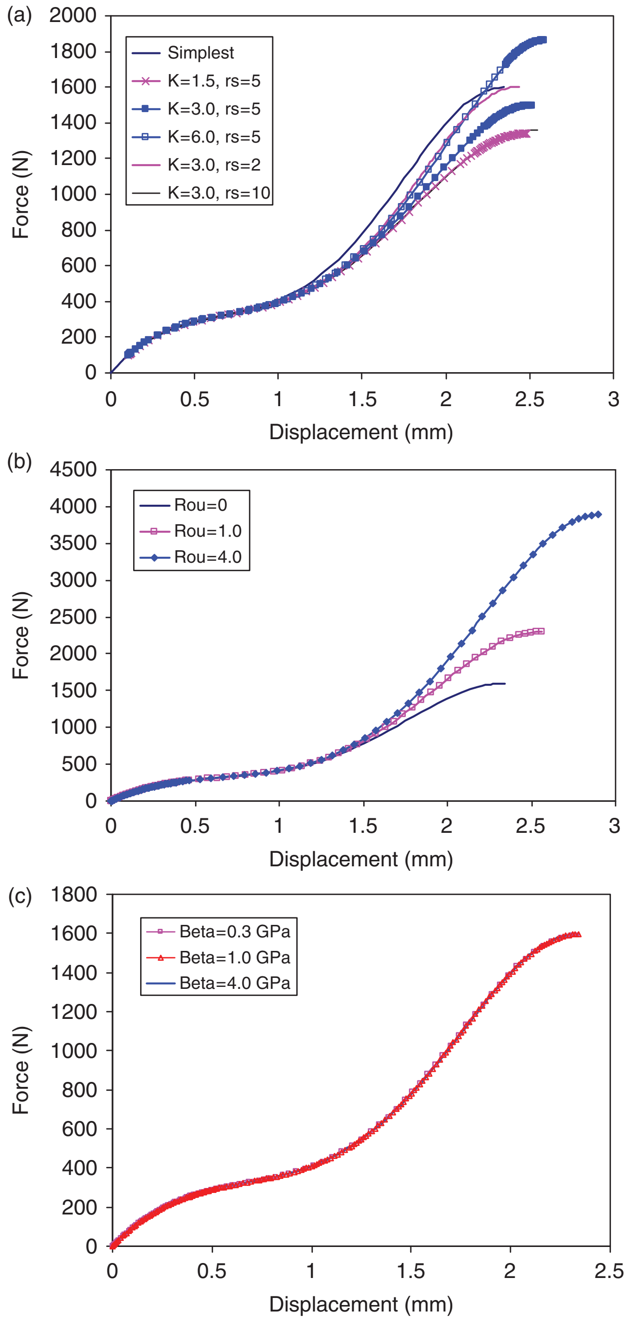

Figure 15. *Investigation of the initial shock stage: (a) the effect of initial yielding the ER fluid; (b) the inertia effect; (c) influence of the fluid compressibility.*

Figure 15(b) shows the dynamic responses of the initial shock stage with three fluid densities applied. It can be seen that the fluid inertia effect greatly influences the initial peak force, and larger the density of the fluid, the higher the initial peak force will be. In addition, three values of the bulk modulus of the fluid were examined, and the results in Figure 15(c) show that the influence of the fluid compressibility is smaller than 0.5%. It should be noted that the use of the rubber plate

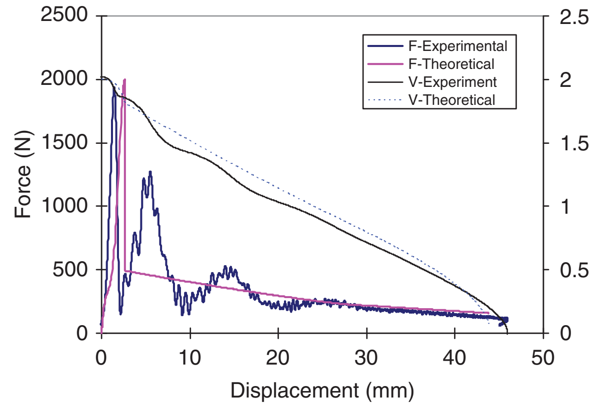

Figure 16. *Comparison between the theoretical analysis and experimental results for the typical dynamic response.*

significantly reduced the influence of the fluid compressibility. Therefore, the compressibility of the ER fluid in this model could be ignored.

The entire predicted response is obtained by using $K_t = 1.5$, $\gamma_S = 2$ and $t_R = 30\,\text{ms}$, and compared with the experimental results in Figure 16. The comparison confirms that the initial peak force can be predicted. Since the vibration and wave propagation within the impinger system are ignored, and also the impinger and piston rod are assumed to move together after they obtained the same velocity, the fluctuations and possible second impact cannot be predicted. After the peak force, the magnitude of the resistant force and final displacement also agree with the experiment very well. It is noted that in the rear part of the loading curve, the theoretical load is over-estimated, which may be because of the fact that in the third impact stage, friction force becomes smaller than that obtained by the quasi-steady tests. However, dynamic measurement of the friction force is still difficult.

The theoretical model is also employed to study the influences of the impact velocity and response time (of the ER fluid to the applied electric field) on the mean crushing force. For given response time $t_R = 30\,\text{ms}$, the mean crushing forces under different impact velocities and different electric field intensities are plotted in Figure 17(a). It reveals that with the increase of the yield stress, the mean crushing force of the dynamic response increases, but at higher impact velocity, this tendency becomes weaker. On the other hand, as shown in Figure 17(b), with the same impact velocity, longer the response time, the smaller the mean crushing force. It should be noted that when the response time approaches to infinite, the mean crushing force approaches under $\tau_Y = 0\,\text{kPa}$. Therefore, the theoretical analysis reveals that with the increase of the impact velocity, the controllability of the ERF cylinder will deteriorate, because of not only the viscous effect, but also the response time.

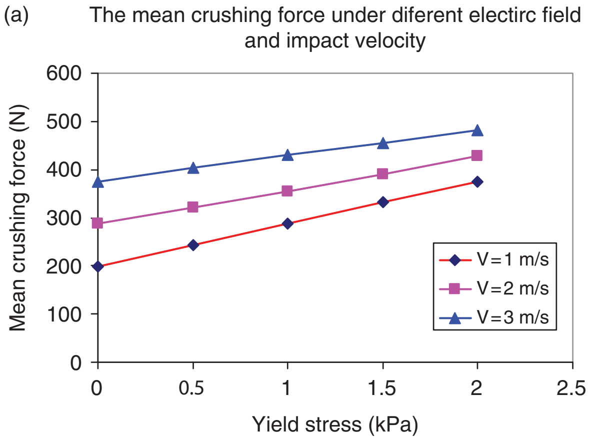

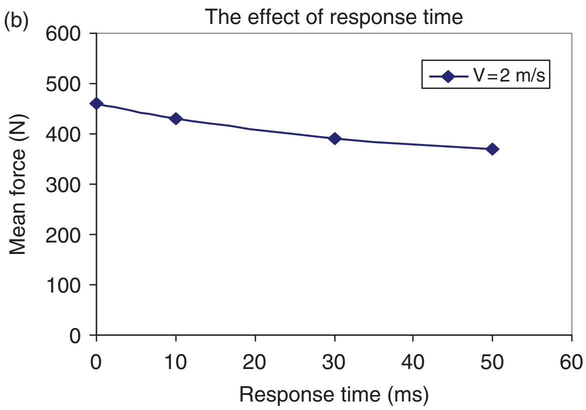

Figure 17. Effects of the yield stress and the response time.

CONCLUDING REMARKS

In this article, the application of ER fluids under impact scenarios is investigated. First, the characterization of ER fluids in parallel duct under high shear rate is discussed, and the errors caused by the nominal and exact methods are analyzed. It is found that although the nominal method can not obtain the accurate viscosity and yield stress, the nominal values can be used to greatly simplify the modeling of the ER devices. Secondly, a double-ended ER cylinder with two coaxial annular ducts was designed and manufactured. Its quasi-steady behavior and dynamic responses under a mass impact are tested. The results show that the dynamic response has three distinct stages, namely, the initial shock stage, a transition stage, and finally the smooth flow stage. The initial shock stage is characterized by a peak force followed by force fluctuations. In the transition stage, two types of ER fluid in the duct are distinguished, namely, the old ER fluid whose yield stress has been fully developed before impact, and new ER fluid with its yield stress partly developed. In this stage, the resistant force of the ER cylinder decreases, but the ER effect is very apparent. After a transition point, the second stage ends and the decrease of the resistant force slows down.

Based on the experimental results, an analytical model is proposed, in which the initial contact, yielding, inertia effect as well as the response time of the ER fluid are all considered. By comparison with the experimental results, it is validated that this model can predict the dynamic response of the ER cylinder well. It is found that the performance of the ER cylinder is mainly determined by the viscous effect, ER effect, and the impact velocity, while the inertia effect and response time of the ER fluid also have some influences. The controllability of the ER cylinder becomes weaker under higher impact velocity, because of the viscous effect and the response time of the ER fluid.

APPENDIX: INFLUENCE OF THE FLUID COMPRESSIBILITY

As shown in Figure A1, when the compressibility of the fluid is concerned, the governing equation of the ER fluid in the lower chamber of this ER cylinder can be expressed by:

$$\frac{\mathrm{d}V}{\mathrm{d}t} + \frac{V}{\beta}\frac{\mathrm{d}P}{\mathrm{d}t} = -Q \tag{A1}$$

where β is the bulk modulus of the ER fluid, V is the volume of the ER fluid in the lower chamber of the cylinder, and Q is the flow rate through the duct. When the piston moves downwards, the ER fluid will flow through the duct into the upper chamber. Hence, the pressure drop through the ER duct can be approximated by:

$$\Delta P = \frac{12\mu LQ}{bh^3} + \frac{2L}{h}\cdot\tau_0, \quad \text{where } \Delta P = P_1 - P_2. \tag{A2}$$

When the compressibility of the ER fluid in the lower chamber is considered, there will be some vacancy in the upper chamber, which means $P_2 = 0$, and $\Delta P = P_1$ (i.e., P). Also, we have the damping force:

$$F_d = P\cdot A_p + F_R \tag{A3}$$

Then, the volume of the lower chamber is:

$$V = (L - x)A_p. \tag{A4}$$

Therefore, the motion equation of the piston is:

$$M\ddot{x} = Mg - P\cdot A_p - F_R, \tag{A5-a}$$

$$P = \frac{12\mu L}{bh^3}\cdot\left[\dot{x} - \frac{(L-x)}{\beta}\times\dot{P}\right]\times A_p + \frac{2L}{h}\cdot\tau_0, \tag{A5-b}$$

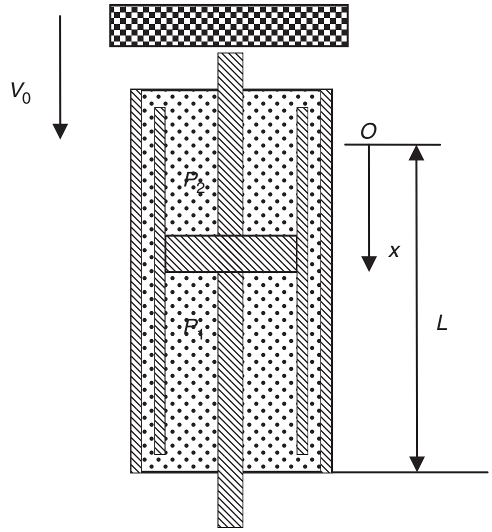

Figure A1. *Cross-section of a typical ER cylinder.*

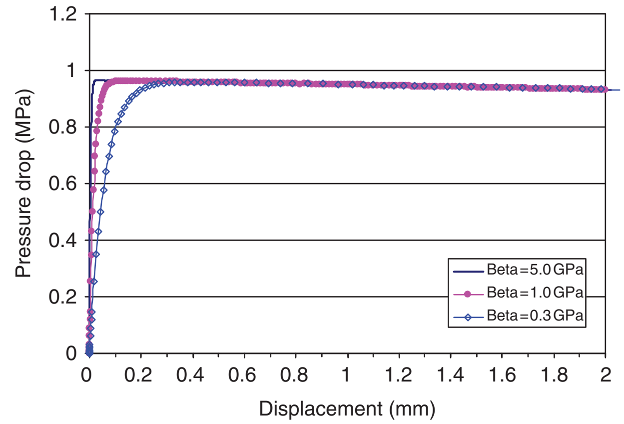

Figure A2. *Dynamic responses of the ER cylinder with different fluid bulk modulus.*

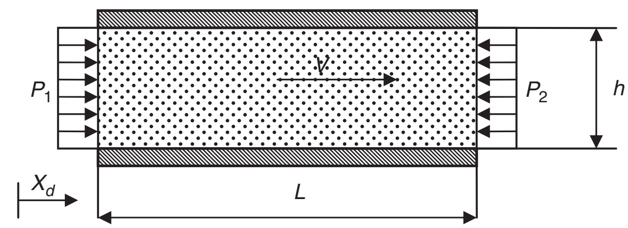

Figure A3. *Flowing of the ER fluid within the duct.*

It can be seen that the first term on the right-hand side of Equation (A5-b) is from the viscous effect, the third term is due to the yield stress or ER effect, while the second term is related to the compressibility of the ER fluid. By means of Equations (A5-a) and (A5-b), for given initial impact conditions, the dynamic response of the ER cylinder can be obtained.

To investigate the influences of the compressibility of the ER fluid, three values of bulk modulus are examined, that is, $\beta = 0.3$, 1.0, 5.0 GPa. The mass of the weight is assumed as $M = 5$ kg, and the impact velocity is $V_0 = 2$ m/s. The geometry of the cylinder is the same as those in the Section 3, while the properties of the ER fluid are $\mu = 0.15$ Pa s, and $\tau_y = 8$ kPa.

Figure A2 plotted the comparison of the dynamic responses with different bulk modulus β. The results showed that the compressibility of the ER fluid only influences the very initial impact stage and nearly does not affect the mean crushing force when the displacement is relatively large. In some degree, the compressibility of ER fluid can explain the gradual increase of the impact force in the initial stage. However, it can not explain the initial peak force which was observed in the experiments.

THE INERTIAL EFFECT OF ER FLUIDS

If the acceleration (or the inertia effect) of the ER fluid is considered, Equation (3) will be incorrect. As shown in Figure A3, the motion equation of the fluid within the duct of length L can be expressed as:

$$(P_1 - P_2) \times bh - 2\tau \times Lb = \rho \ddot{X}_d Lbh, \qquad \text{(A6)}$$

where τ is the shear stress at the two boundaries, x_d is the displacement of the ER fluid in the duct, and b is the width of the duct in the direction normal to this page. Hence, x_d can be obtained by:

$$X_d = \frac{A_p}{bh} \times X. \qquad \text{(A7)}$$

After simplifying Equation (A7), we have:

$$\tau = \Delta P \times \frac{h}{2L} - \frac{\rho h}{2} \times \frac{A_p}{bh} \times \ddot{X}. \qquad \text{(A8)}$$

If the inertial effect of the fluid (i.e., the second term on the right-hand side of the equation) is ignored, Equation (A8) can be simplified to Equation (3) in this article.

Recalling Equation (11) in the article, the pressure drop can be approximated as:

$$P = \frac{2L}{h} \cdot \left[\frac{6\mu}{bh^2} \cdot \dot{X} \times A_p + \tau_0 + \frac{1}{2} \times \rho h \cdot \frac{A_p}{bh} \times \ddot{X} \right]. \qquad \text{(A9)}$$

By combining Equation (A5-a), we have:

$$\left(M + \rho \cdot LA_p \times \frac{A_p}{bh} \right) \ddot{X} = Mg - \left(A_p \times \frac{12\mu L}{bh^3} \cdot \dot{X} + \frac{2L}{h} \tau_0 \right) \cdot A_p - F_R. \qquad \text{(A10)}$$

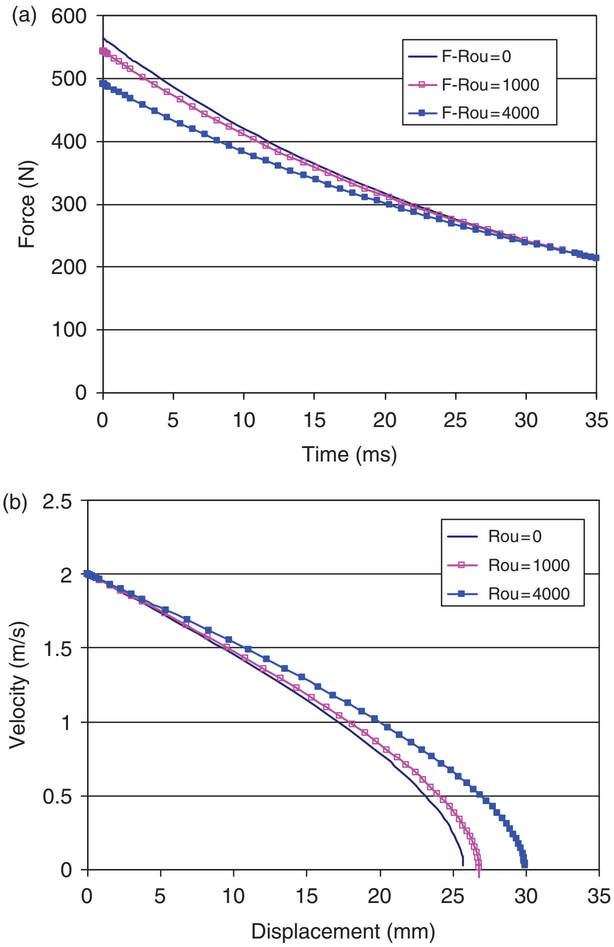

***Figure A4.** Investigation of the inertia effect of the ER fluid.*

According to the above equation, the inertia effect of ER fluid can be evaluated by the mass ratio $\rho L A_p^2/(M \times bh)$. If this ratio is small enough, the inertia effect can be ignored. By using $\rho = 1.0 \times 10^3\,\mathrm{kg/m^3}$, $L = 65\,\mathrm{mm}$, $A_p = 1206\,\mathrm{mm^2}$, $M = 5\,\mathrm{kg}$, this mass ratio is about 0.04.

To further investigate the influence of the ER fluid inertial effect, an impact response is analyzed by means of Equation (A10). The geometric and impact conditions are the same with those for the investigation of compressibility, and the dynamic responses of the ER cylinder under $\rho = 1.0 \times 10^3$ and $4 \times 10^3\,\mathrm{kg/m^3}$, with $V_0 = 2\,\mathrm{m/s}$, were analyzed. The force history and velocity-displacement relations for different ρ are shown in Figure A4(a) and (b), in which $\rho = 0$ means the inertia effect is ignored. It is seen that larger the velocity, the more serious the influence of the inertia effect will be. For $\rho = 1.0 \times 10^3\,\mathrm{kg/m^3}$, the influence of the resistant force at the very beginning is about 4%, which agrees well with the estimation in the previous paragraph. However, when the density of the fluid is $\rho = 4.0 \times 10^3\,\mathrm{kg/m^3}$, the influence of the inertia effect will be significant.

ACKNOWLEDGEMENTS

This study is supported by the Hong Kong Research Grant Council (RGC) under CERG grant No.621505 and the National Natural Science Foundation of China under Key Project No.10532020. Their financial supports are gratefully acknowledged. The authors also would like to thank C.B. Zhang, Alex Fok, J.B. Wu and X.Q. Gong for their help.

REFERENCES

Ahmadian, M. and Norris, J.A. 2004. "Rheological Controllability of Double-ended MR Dampers Subjected to Impact Loading," In: Wang, K.-W. (ed.), *Proceedings of SPIE*, 15 March, San Diego, CA, Volume 5386 – Smart Structures and Materials*,* 2004: Damping and Isolation.

Ahmadian, M. and Norris, J.A. 2008. "Experimental Analysis of Magneto-rheological Dampers when Subjected to Impact and Shock Loading," *Communication in Nonlinear Science and Numerical Simulation*, 13:1978–1985.

Batterbee, D.C., Sims, N.D., Stanway, R. and Wolejsza, Z. 2007a. "Magneto-rheological Landing Gear: 1. A Design Methodology," *Smart materials and Structures*, 16:2429–2440.

Batterbee, D.C., Sims, N.D., Stanway, R. and Rennison, M. 2007b. "Magneto-rheological Landing Gear: 2. Validation Using Experimental Data," *Smart Materials and Structures*, 16:2441–2452.

Chen, S.M. and Wei, C.G. 2006. "Experimental Study of the Rheological Behavior of Electro-rheological Fluids," *Smart Materials and Structures*, 15:377.

Choi, S.B. and Lee, D.Y. 2005. "Rotational Motion Control of a Washing Machine using Electro-rheological Clutches and Brakes," *Proceedings of the Institution of Mechanical Engineers, Part C: Journal of Mechanical Engineering Science*, 219:627–637.

Choi, Y.T., Cho, J.U., Choi, S.B. and Wereley, N.M. 2005. "Constitutive Models of Electro-rheological and Magneto-rheological Fluids using Viscometers," *Smart Materials and Structures*, 14:1025–1036.

El-Wahed, A.K., Sproston, J.L. and Schleyer, G.K. 1999. "A Comparison Between Electro-rheological and Magneto-rheological Fluids Subjected to Impulsive Loads," *Journal of Intelligent Materials Systems and Structures*, 10:695–700.

Ferguson, J. and Kemblowski, Z. 1991. *Applied Fluid Rheology*, Elsevier Applied Science, London.

Goncalves, F.D., Ahmadian, M. and Carlson, J.D. 2006. "Investigating the Magneto-rheological Effect at High Flow Velocities," *Smart Materials and Structures*, 15:75–85.

Lee, D.Y., Choi, Y.T. and Wereley, N.M. 2002. "Performance Analysis of ER/MR Impact Damper Systems using Herschel-Bulkley Model," *Journal of Intelligent Materials Systems and Structures*, 13:525–531.

Makris, N., Burton, S.A. and Taylor, D.P. 1996. "Electro-rheological Damper with Annular Ducts for Seismic Protection Applications," *Smart Materials and Structures*, 5:551–564.

Nam, Y.J. and Park, M.K. 2007. "Performance Evaluation of Two Different Bypass-type MR Shock Dampers," *Journal of Intelligent Materials Systems and Structures*, 18:707–717.

Nouar, C. and Frigaard, I.A. 2001. "Nonlinear Stability of Poiseuille Flow of Bingham Fluid Theoretical Results and Comparison with Phenomenological Criteria," *Journal of Non-Newtonian Fluid Mechanics*, 100:127–149.

Park, W.C., Choi, S.B. and Suh, M.S. 1999. "Material Characteristics of an ER Fluid and its Influence on Damping Forces of an ER Damper Part I: Mechanical Properties," *Materials and Design*, 20:317–323.

Song, H.J., Choi, S.B., Kim, J.H. and Kim, K.S. 2002. "Performance Evaluation of ER Shock Damper Subjected to Impulsive

Excitation," *Journal of Intelligent Materials Systems and Structures*, 13:625–628.

Stanway, R. 2004. "Smart Fluid: Current and Future Developments," *Materials Science and Technology*, 20:931–939.

Stanway, R., Sproston, J.L. and EI-Wahed, A.K. 1996. "Applications of Electro-rheological Fluids in Vibration Control: a Survey," *Smart Materials and Structures*, 5:464–482.

Wang, J. and Meng, G. 2001. "Magneto-rheological Fluid Devices and their Applications in Mechanical Engineering," *Journal of Mechanical Strength*, 23:50–56.

Wen, W.J., Huang, X.X. and Sheng, P. 2004. "Particle Size Scaling of the Giant Electro-rheological Effect," *Applied Physics Letters*, 85:299–301.

Yeo, M.S., Lee, H.G. and Kim, M.C. 2002. "A Study on the Performance Estimation of Semi-active Suspension System considering the Response Time of Electro-rheological Fluid," *Journal of Intelligent Material Systems and Structures*, 13:485–489.

Zhang, X.W., Zhang, C.B., Yu, T.X. and Wen, W.J. 2008. "Characterization of Electro-rheological Fluids under High Shear Rate in Parallel Ducts," *International Journal of Modern Physics B*, 22:6029–6036.